Imran Ali, Changsheng Peng*, Dichu Lin and Iffat Naz*

Green synthesis of the innovative super paramagnetic nanoparticles from the leaves extract of *Fraxinus chinensis Roxb* and their application for the decolourisation of toxic dyes

https://doi.org/10.1515/gps-2018-0078
Received April 10, 2018; accepted June 20, 2018; previously published online July 14, 2018

Abstract: The leaves extract of *Fraxinus chinensis Roxb* was used for the synthesis of the innovative phytogenic magnetic nanoparticles (PMNPs) without adding toxic surfactants. The formation, morphology, elemental composition, size, thermal stability, structure and magnetic properties of these PMNPs were examined by UV-visible spectrophotometry, FT-IR, XRD, SEM, EDX, TEM, VSM, XPS, BET and TGA. The reactivity of the obtained PMNPs against decolourising toxic dyes, namely, malachite green (MG), crystal violet (CV) and methylene blue (MB), were investigated by UV-vis spectrophotometry. Further, the factors affecting the removal of dyes, including solution pH, adsorbent dosages, initial concentration of dyes, reaction temperature and contact time, were also investigated. The results revealed the decolourisation of 99.12% of MG and 98.23% of CV within 60 min, and 97.52% of MB within 200 min by the PMNPs using dyes concentration of 25 mg/l at pH 6.5 and 298.15 K. The kinetics outcome indicated that the degradation of dyes matched well to the pseudo first-order reaction kinetics model. Furthermore, the probable degradation mechanism of dyes by the PMNPs, including the adsorption of cationic dye molecules onto the negatively charged surface of adsorbent and the oxidation of the Fe° in the solution, were discussed. Thus, the PMNPs can be produced by the bulk and have great potential to be employed for biomedical/environmental remediation.

***Corresponding authors: Changsheng Peng,** The Key Lab of Marine Environmental Science and Ecology, Ministry of Education, Ocean University of China, Qingdao 266100, China; and School of Environmental and Chemical Engineering, Zhaoqing University, Zhaoqing 526061, China, e-mail: pcs005@ouc.edu.cn, cspeng@ouc.edu.cn; and **Iffat Naz,** Department of Biology, Scientific Unit, Deanship of Educational Services, Qassim University, Buraidah 51452, Kingdom of Saudi Arabia (KSA), e-mail: iffatkhattak@yahoo.com. https://orcid.org/0000-0002-6711-0189
Imran Ali: Department of Environmental Engineering, College of Environmental Science and Engineering, Ocean University of China, Qingdao 266100, China
Dichu Lin: The Key Lab of Marine Environmental Science and Ecology, Ministry of Education, Ocean University of China, Qingdao 266100, China

Keywords: decolourisation; *Fraxinus chinensis Roxb*; phytochemical characterisation; phytogenic magnetic nanoparticles; plant leaves extract; toxic dyes.

1 Introduction

Currently, the demand for nanoparticles (NPs) has significantly increased for optical, electrical, chemical, biomedical and environmental protection applications, due to their unique size, shape and surface properties [1–3]. Thus, magnetic nanoparticles (MNPs) are gaining tremendous attention owing to their magnetic behaviour [4]. The demand for MNPs for modern applications has also increased, such as those for targeted drug delivery, magnetic resonance imaging (MRI), lithium ion batteries, tissue-repair engineering, spintronics, catalysis, adsorption of pollutants and the recovery of toxic metals from soil and waters [5–12]. In these circumstances, MNPs have been produced by various techniques (i.e. physical, chemical and biological routes) [13]. However, the physical and chemical approaches are facing serious complications due to the high fabrication costs and the prerequisite of highly toxic/reactive reducing agents (e.g. sodium borohydride, hydrazine, etc.), which have led to restrictions in their commercial applications [14, 15]. In addition, the agglomeration of MNPs limit their applications, particularly in the biomedical applications to deliver targeted genes or drugs into the desired locations because of the presence of the Van-der Wall and magnetic forces. Similarly, the aggregation of MNPs reduces their performance for possible environmental protections applications [16, 17]. Meanwhile, the utilisation of highly toxic surfactants or soluble polymers onto the MNPs to inhibit this aggregation are eventually increasing threats to the environment by generating secondary pollutants in the form of by-products [18]. Hence, there is a need to develop an alternate efficient method for the fabrication of MNPs with desirable quality [19–21]. In relation to such a demand, green nanotechnology has kept pace to handle this situation.

Green nanotechnology is based on the concept of green chemistry, and it is a branch of science dealing with the design, development and execution of chemicals and

processes to minimise the employment and production of hazardous substances that can harm human health and the surrounding environment [2, 22]. In the fabrication of MNPs, green chemistry mainly follows the following steps: the selection of (a) environmental friendly solvents, (b) safe and non-toxic reducing agents and (c) non-toxic and biodegradable capping agents or dispersing agents [22–26]. Hence, there is an increasing research interest to explore and identify cheap, biocompatible and chemically stable but environmental friendly biomaterials, which can be used as both reducing and capping agent to fabricate MNPs [24]. Following these guidelines, exploring the capability of plants in the fabrication of MNPs has become an innovative approach to develop these nano-materials [27, 28]. Plants are comparatively better options in producing MNPs than microbes, which demand costly instrumentations to produce MNPs. In addition, the presence of chemicals (i.e. sugars and antioxidants) play a very important role in reducing metal ions in the absence of other chemicals. Various kinds of plants and plant's parts have been successfully utilised in the production of MNPs, the details of which are given in previously published reports [2, 29–31].

Herein, we report for first time, the successful green production of phytogenic magnetic nanoparticles (PMNPs) from the leaves extract of *Fraxinus chinensis Roxb*. The *F. chinensis Roxb*, commonly known as "Chinese ash", is a species of flowering trees, whose leaves are used in traditional Chinese medicine for dysentery disorders. This genus is widespread across much of Europe, Asia and North America. The leaves extract of *F. chinensis Roxb* mainly contained polyphenols that are non-toxic, biodegradable and water soluble at room temperature. Further, polyphenols can make complexes with metal ions and then reduce and stabilise these metal ions to form MNPs. Therefore, the following core objectives were designed in the study: (i) to optimise the extraction conditions to obtain the highest antioxidant capacity by varying pertaining factors (i.e. pH, temperature, contact time, shaking speed and mass of plant leafs per ml of water/solvent); (ii) to fabricate the PMNPs using the optimised conditions; (iii) to characterise the fabricated PMNPs by using different techniques (i.e. UV-vis spectra, FTIR, powder XRD, TEM, BET, TGA, SEM, EDX XPS and VSM); (iv) to investigate its reactivity against decolourising toxic dyes, including malachite green (MG), crystal violet (CV) and methylene blue (MB) by UV-vis spectrophotometry; (iv) to examine influence of various operating parameters on the removal of dyes, including solution pH, adsorbent dosages, initial concentration of dyes, reaction temperature and contact time; and (v) to employ pseudo first-order kinetic model for exploring probable degradation mechanism of the suggested dyes by PMNPs.

2 Materials and methods

2.1 Instrumentation and chemicals

In the present research, different instruments, such as Atomic absorption spectrometry (Solaar M6, Thermo Elemental, USA), muffle furnace (HMX-1400, Shanghai HaoYue), pH meter (mV/ORP METTLER TOLEDO), rotary shaker (THZ-92A, China), elemental analyser (EA, Vario EL cube, German), UV-vis spectrophotometer, magnetic stirrer, centrifuge machine, thermostatic water bath shaker, weighing balance, Erlenmeyer flasks and volumetric flasks were used to conduct all the experiments. For the characterisation, Fourier-transform infrared spectroscopy (FTIR, Bruker Vertex 70), scanning electron microscope with integrated energy dispersive X-ray system (SEM-EDX, JSM-6610 LV, Japan Electronics), X-ray diffractometer (XRD, Philips Electronic Instruments), thermo-gravimetric analyser (TGA, NETZSCH TG 209F3), Brunauer-Emmet-Teller (BET) analyser and vibrating sample magnetometer (VSM, VSM600) were employed.

Various different chemicals, including ferric chloride hexahydrate ($FeCl_3 \cdot 6H_2O$), acetate buffer, ferrous sulfate ($FeSO_4 \cdot 7H_2O$), copper sulfate, sodium hydroxide (NaOH), $MgSO_4$, HCl, potassium ferricyanide, ferric trichloride, $NaBH_4$ and Na_2CO_3 (Aldrich, 99%), ethanol (C_2H_5OH), gallic acid (Merck, 99.9%), tripyridyltriazine (TPTZ, HPLC grade, Anaqua, 99.9%), malachite green ($C_{23}H_{25}ClN_2$), crystal violet ($C_{25}H_{30}ClN_3$) and methylene blue ($C1_6H_{18}ClN_3S$) (Merck, 99.9%) were used without further purification in the current research. Deionized (DI) water was obtained from the Qingdao water purification agency and was used to prepare all aqueous solutions for all experimentation.

2.2 Green production of the PMNPs

2.2.1 Selection of the leaves of *F. chinensis Roxb*: For the fabrication of the PMNPs, the *F. chinensis Roxb* samples were selected and the leaves were collected from a flower market near the Ocean University of China, Qingdao, China. The leaves were washed thoroughly with DI water to remove impurities like dust. After washing, the leaves were allowed to dry under sunlight for at least 10 days and oven dried for 6 h at 385.15 K to reduce the moisture contents. Thereafter, the dried leaves were manually chopped into small pieces and passed through a 2 mm sieve. Finally, the sieved product was collected and stored for further use in the preparation of the extract.

2.3 Optimisation of extraction protocol

2.3.1 Evaluation of the reducing capacity of *F. chinensis Roxb* leaves extract: The reducing ability of the leaves extract of *F. chinensis Roxb* was investigated using the ferric reducing antioxidant power (FRAP) assay and colour development tests, as described by Manquián-Cerda et al. [32]. During the FRAP assay, the ability of the plant extract (PE), to reduce Fe^{+3} to Fe^{+2} was measured at absorbance ($\lambda = 593$ nm) by producing blue complex with TPTZ. The FRAP reagent was made by

using 20 mM of $FeCl_3$ solution, 300 mM of acetate buffer and 10 mM of TPTZ solution in HCl at a 1:1:10 ratio. The absorbance of samples containing 800 µl of FRAP reagent, 60 µl of H_2O, and 20 µl of extract was determined at $\lambda = 593$ nm by UV-vis spectrophotometer. The FRAP reagent was kept at room temperature (298.15 K) throughout the experiments. The standard calibration curve for this test was also designed using six Fe^{+2} standards, with concentrations ranging between 100 and 1000 µmol/l ($r > 0.999$), which were further used in extract optimisation study. In addition, different colour development tests were used to investigate the presence of probable organic contents in the plant extract, which can reduce Fe^{+3} to Fe^{+2}. For this purpose, ferric trichloride-potassium ferricyanide, HCl-Mg reaction and alkaline copper sulfate tests were employed according to Wei et al. [34].

2.3.2 Evaluation of the total phenolic content (TPC) in the leaves extract of *F. chinensis Roxb*: The presence of phenolic compounds is often considered an important element in the formation of green MNPs, because it has been reported that phenolic compounds with –OH groups in the orhoposition assist in the reduction and construction of green MNPs [33]. For this purpose, the Folin-Ciocalteu method was employed to investigate the TPC in the plant extract using gallic acid as the standard [34]. A dilution sample was prepared containing plant extract (20 µl) and 40 µl of pure DI water. Then, the Folin-Ciocalteu reagent (100 µl) was added and mixed for 5 min, after which 300 ml of Na_2CO_3 solution was injected and permitted to stand for 15 min. Finally, the absorbance of the sample was determined at $\lambda = 765$ nm by UV-vis spectrophotometer. The results of the TPC were stated as milligrams of gallic acid equivalent (GAE) per gram of dry weight.

2.3.3 Optimisation of the extraction conditions: To determine the best conditions for maximum extraction with high antioxidant capacities, the extraction optimisation studies were conducted. The FRAP assay was used to calculate the antioxidant capacity of the extract. For optimisation studies, such factors as mass of leaves and solvent volume ratio, contact time, temperature and pH, were optimised. The mass of leaves: solvent volume ratio experiments were conducted with different masses of the selected leaves (from 1 to 12 g) using 80 ml of DI water; the range of contact time was 20–120 min, the range of temperature was 298.15 K–473.15 K and pH range was 2–12. The pH levels of the samples were maintained using 0.1 mol/l NaOH and HCl. At the end of each experiment, the leaves extract was centrifuged for 20 min at 8000 rpm, after which the supernatant was filtered through a 0.22 µm filter paper and then 20 µl of extract was used in the FRAP assay. The standard calibration curve (as described above) was employed to obtain the real value of the antioxidant capacity, and all the tests were commenced in triplicate.

2.4 Fabrication of the PMNPs

For the fabrication of the PMNPS, the optimum extraction condition was selected and 10 g of the powdered *F. chinensis Roxb* leaves was added into 80 ml of DI water, and then the mixture was heated at 353.15 K for 90 min. The pH of the solution was maintained at three using 0.1 mol/l NaOH and HCl solution. Then, the MS (1:1) ratio of (Fe^{+2}:Fe^{+3}) was prepared using 50 ml DI water; next, 50:50 (vol./vol.) ratio of MS and PE was prepared and boiled at 353.15 K with continuous stirring (100 rpm) by a magnetic stirrer heater for 60 min. The pH of the mixture was adjusted at 12 using 0.1 mol/l NaOH solution added drop-wise until the mixture colour changed from reddish brown to black, thus indicating the formation of PMNPs. Then, the mixture was allowed to settle down for 60 min and then the black colour precipitations were centrifuged for 20 min at 8000 rpm. The supernatant was vacuum-filtered through a 0.22 µm filter paper, after which the black powder was collected and washed twice with 50 ml of ethanol solution. Further, the final product was again vacuum-filtered through a 0.22 µm filter paper and the collected black powder was oven-dried for at least 120 min at 353.15 K.

2.5 Characterisation of the *F. chinensis Roxb* extract and the PMNPs

The elemental contents (e.g. C, N, S and H) and the heavy metals content of the leaves extract were determined by using an elemental analyser and atomic absorption spectrometry, respectively. Further, the fabricated PMNPs were characterised using FTIR, XRD, SEM, EDX/S, TEM, XPS, TGA, VSM and BET techniques. A Bruker Vertex 70 was used for the FTIR analysis. Next, the probable bio-molecules present in the extract were identified, which were responsible for the reduction and stabilisation of PMNPs. A Philips Electronic Instrument was employed for the XRD analysis, and the crystalline shape of the fabricated PMNPs was identified. The fabricated PMNPs sample was washed completely with ethanol prior to the analysis, in order to minimise the NaCl content and other impurities that crystallised out during the fabrication process. The samples were scanned within 2θ range of 20°–70°. The morphologies of the fabricated PMNPs were examined by SEM and TEM. The elemental content was analysed by energy dispersive spectroscopy EDS/X. Further, X-ray photoelectron spectrum was also used to identify the elemental composition. The thermal stability of the PMNPs was estimated by the TGA, and the NETZSCH TG 209F3 instrument was employed with a heating rate of 283.15 K/min in the temperature range of 303.15 K–1073.15 K under nitrogen gas (flow rate, 20 ml/min). The magnetic measurements of the PMNPs were done at 300 K temperature through a VSM by applying a magnetic field of up to 15kOe. The surface properties of the prepared material were determined using BET method at temperature 77 K using nitrogen gas.

2.6 Experiments for the decolourisation of toxic dyes by the PMNPs

In order to evaluate the reactivity and effectiveness of the fabricated PMNPs, cationic toxic dyes [i.e. malachite green (MG), crystal violet (CV) and methylene blue (MB)] were selected for the degradation experiments, and their removal efficiencies were compared. All the experiments were conducted in batch mode by shaking Erlenmeyer flasks in a temperature-controlled rotary shaker under atmospheric pressure and room temperature (298.15 K) by adjusting the shaking speed at 100 rpm. A fixed amount of 0.3 g/l powdered PMNPs was added in to 40 ml of the aqueous solution containing 25 mg/l of MG, CV and MB solutions, respectively. The pH levels of these dyes solutions were maintained at 6.5 unless otherwise stated. The pH adjustments were made using 0.1 mol/l NaOH and HCl solution depending on the requirement. Initially, various influencing parameters were

investigated, including adsorbent dosages (0.05–1.5 g/l), solution pH (2–12), initial dyes concentration (25–1000 mg/l), contact time (0–220 min) and temperature (298.15 K–333.15 K). Following this, the mixtures were centrifuged at 10,000 rpm for 15 min, and then the liquid supernatant was collected to determine the final concentration of the dyes. The absorbance rates of the dye solutions were measured using UV-vis spectrophotometer at $\lambda_{max} = 617$ nm (MG), $\lambda_{max} = 585$ nm (CV) and $\lambda_{max} = 664$ nm (MB). Finally, the removal/degradation efficiency of the selected dyes by PMNPs at different time interval was calculated using the equation

$$\text{Removal efficiency (\%)} = \frac{C_o - C_t}{C_o} \times 100\%,$$

where C_o (mg/l) is the initial dye concentration in the solution and C_t (mg/l) is the final dye concentration in the solution at different time intervals.

3 Results and discussion

3.1 Characterisation of the leaves extract of *F. chinensis Roxb*

The main objective of characterising the leaves extract of *F. chinensis Roxb* was to examine the safe and clean green synthesis of PMNPs through an investigation of the elemental and heavy metal contents. The surplus amount of heavy metals can generate contamination in the leaves extract. In addition, it has been reported that, by identifying the elemental contents (e.g. C, H, N and S), the probability regarding the presence of certain organic compounds can be supposed. In the present study, the elemental contents of *F. chinensis Roxb* were C (38.6%), H (4.99%), S (0.39%) and N (4.38%). These results indicate that the presence of N and S might be due to protein, chlorophyll, nucleic acids, cysteine, cystine and methionine in the leaves extract. In contrast, the negligible contents of heavy metals [Cr (0.011 mg/l), Fe (0.06 mg/l), Pb (0.07 mg/l), Co (0.013 mg/l), Cd (0.001 mg/l) and Zn (0.25 mg/l)] were also observed in the extract. Our findings indicate that organic compounds are mainly found in the extract, whilst only negligible amounts of heavy metals contents were observed, thus confirming the safe and green fabrication of PMNPs.

3.2 Optimisation of the leaves extraction protocol

In the present research, the main purpose of optimising the extraction protocol was to find out the maximum leaf extraction with high antioxidant capacities (Figure 1). These findings showed that, by increasing the mass of leaves into the extract solution, the antioxidant capacities initially increased (from 0.043 to 0.047 Fe^{+2} mmol/l), but after increasing the mass of leaves by 10 g, the antioxidant capacity was almost stable (Figure 1A). Hence, from an economical point of view and due to the high antioxidant capacity, we selected 10 g/80 ml as the optimal mass of leaves for further studies. After this, by increasing the temperature (from 298.15 K to 393.15 K), the antioxidant capacity also initially increased (from 0.041 to 0.044 Fe^{+2} mmol/l) and then gradually decreased by the increasing temperature. However, almost a stable value of 0.044 ± 0.001 Fe^{+2} mmol/l was observed between 353.15 K to 423.15 K (Figure 1B). Hence, for the purpose of green fabrication, 353.15 K was selected as an optimal temperature for further studies. At this temperature, the contact time varied from 20 to 120 min.

The abovementioned findings illustrated that, by increasing contact time (from 20 to 90 min), the antioxidant capacities initially increased (from 0.041 to 0.046 Fe^{+2} mmol/l) and then decreased between 90 to 120 min. This reduction of antioxidant capacities might be due to the oxidation of antioxidant chemicals through the exposure of air, according to the findings of Wei et al. [34]. Hence, 90 min was chosen as the optimal contact time (Figure 1C). Initially, the pH of the extract was 5.56 and it was adjusted by using 0.1 mol/l NaOH and HCl solution. The findings of the current study showed that the antioxidant capacities declined from 0.048 to 0.044 Fe^{+2} mmol/l with increasing pH and then became almost stable after pH 9. Therefore, according to our findings, pH 3 was selected as the optimal pH for further studies (Figure 1D). Furthermore, we also noticed that, at optimised conditions, higher antioxidant capacity (0.047 Fe^{+2} mmol/l) and TPC (83.3 ± 5.1 GAE mg/g DW) were measured by the FRAP and the Folin-Ciocalteu method. These findings illustrated that the *F. chinensis Roxb* leaves extract contained high amounts of reducing compounds, which could produce a higher yield of PMNPs. Similarly, we also observed this by colour development tests, and all the findings are shown in Table 1. Moreover, Wei et al. [34] also reported that, when plant extracts have higher antioxidant capacity and TPC, then they have higher potential in producing PMNPs through the reduction of metal ions.

3.3 Characterisation of the PMNPs

3.3.1 UV-vis spectra analysis

The fabricated PMNPs were first confirmed by change in colour from dark green to black using UV-vis absorption spectra. Figure 2 illustrates that the reaction between

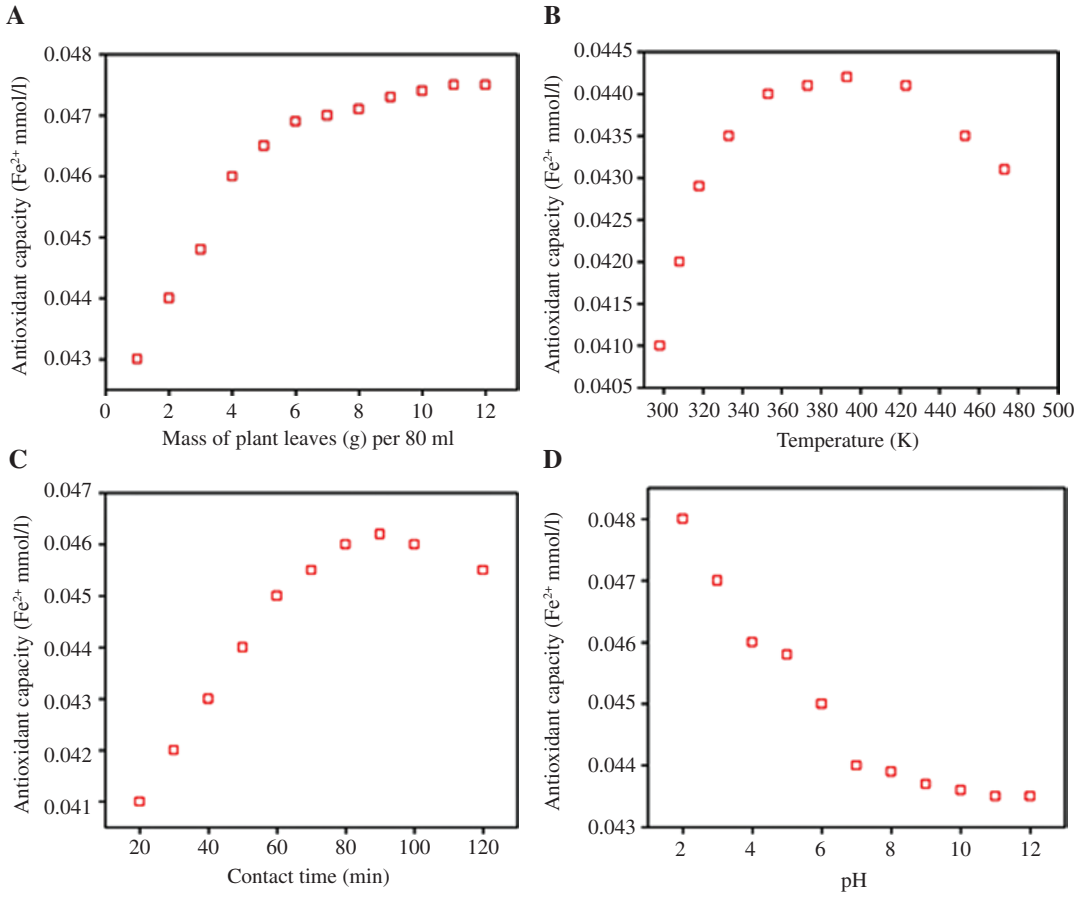

Figure 1: The results of the influencing factors for the optimisation of extraction conditions on the basis of antioxidant capacity (Fe^{3+} mmol/l) (A) mass of plant leaves (g) per 80 ml (B) temperature (K) (C) contact time (min) and (D) pH.

Table 1: The colour development tests to investigate the presence of organic contents in the leaves extract of *Fraxinus chinensis Roxb*.

Tests	Development of colour	Development of precipitation	Indications
Ferric trichloride-potassium ferricyanide	Blue-green spots on the filter paper	No after adding gelatin	Presence of phenolic compounds and tannins in the extract
HCl-Mg reaction	Solution colour changed to reddish brown	No	Presence of flavonoid in the extract
Alkaline copper sulfate	Red	Red copper oxide precipitation appeared	Presence of reducing sugar in the extract

metal salt and leaves extract was instantaneous and the colour of the reaction solution changed from dark green to black. This fabrication might be due to a variety of plant bio-molecules (polyphenols), which played a major role in the reduction of metal ions and the sufficiently stabilisation of the Fe_3O_4 NPs to fabricate PMNPs under an alkaline condition (pH 12). Thus, after the reaction, it can be seen that the UV spectra of the fabricated PMNPs had broad absorption at a higher wavelength than the plant extract and there was no sharp absorption at a lower wavelength (Figure 2A and B). Finally, 3-MPA incorporated on the surface of the PMNPs in an alkaline medium (pH 8). The formation of the PMNPs and 3-MPA capped PMNPs or the reactions that might have occurred in the preparation can be summarised below.

$$FeSO_4 \cdot 7H_2O + 2FeCl_3 \cdot 6H_2O + 8NaOH \xrightarrow{\Delta} Fe_3O_4 + 6NaCl + (Na)_2SO_4 + 17H_2O$$

$$Fe_3O_4 + \text{Plant extract} + 17H_2O \xrightarrow{\Delta} \text{Plant extract} - Fe_3O_4 / \text{PMNPs}$$

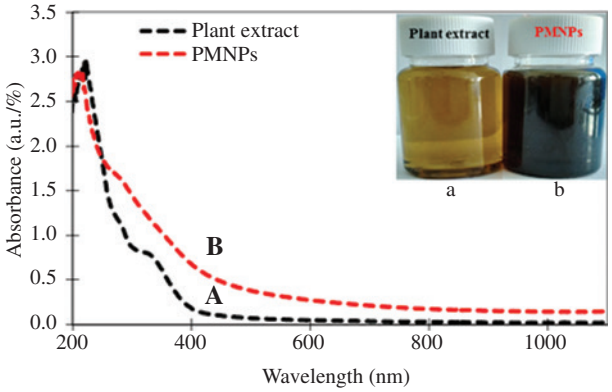

Figure 2: The UV-vis spectra of the (A) plant extract and (B) phytogenic magnetic nanoparticles (PMNPs); inset shows the photographic interpretation of the reaction (Reproduced from Ali et al. 2018 with permission from Royal Society of Chemistry, UK).

3.3.2 FTIR analysis

Figure 3 demonstrates the FTIR spectra of *F. chinensis Roxb* leaves extract for the fabrication of PMNPs. The FTIR spectra revealed different peaks in the spectral range of 500–4000 cm^{-1}, and these peaks were probably due to the presence of plant bio-molecules (polyphenols) on the surface of PMNPs. Figure 3 also shows the board absorptions at 3454 cm^{-1}, mainly representing the O-H stretching vibrations (polyphenolic group) and shifting to 3460 cm^{-1} (Figure 3B). Its breadth might be due to the formation of intra and intermolecular hydrogen bonds [35]. The peaks at 2935 and 2893 cm^{-1} represent the O-H stretching and C-H stretching vibrations, respectively, of carboxylic acid, alcohol or alkene (Figure 3B). A very strong peak at 1662 cm^{-1} revealed the presence of C=O stretching or C=C stretching vibration of the acid derivatives; this shifted to 1639 cm^{-1}. These peaks might indicate the sign of physisorbed or chemisorbed H_2O on the PMNPs, as previously reported by various scientists [35, 36]. A slightly broad absorption peak at 1163 cm^{-1} indicated the C-O stretching vibration of ester, and this shifted to 1114 cm^{-1}, thereby indicating the C-O stretching vibration of aliphatic ether or bond of glucose ring in the extract. Moreover, after the reduction of metal salt solution, the prompt decrease in the intensity at 1662 and 1163 cm^{-1} imply the major role of the –OH group in this reduction process, as previously discussed by various investigators [18, 35]. Finally, a strong absorption band at 585 cm^{-1} can be attributed to the characteristic band of Fe-O, thus suggesting the formation of Fe_3O_4 NPs or PMNPs, as reported by Prasad et al. [36]. Therefore, the FTIR results verified the capping and involvement of plant bio-molecules (polyphenol, carboxyl, glucose, alkene, primary amine, ester, aliphatic and ether) on the surface of the PMNPs in the shape of the –OH, C-H, C-O functional groups. In addition, the FTIR results were also verified by the results obtained from the colour development tests (as discussed in the extract characterisation section).

3.3.3 Powder XRD analysis

Figure 4 shows the XRD pattern of the PMNP structure. The reflections in the XRD diagram belong to iron oxide, magnetite (Fe_3O_4) or ferric oxide orhematite (Fe_2O_3), in addition

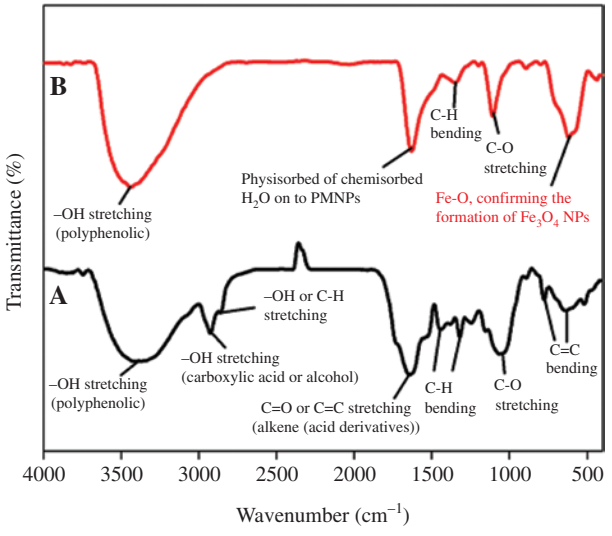

Figure 3: The Fourier transform infrared (FTIR) spectrum of (A) plant extract; (B) fabricated phytogenic magnetic nanoparticles (PMNPs). Reproduced from Ali et al. (2018) with permission from Royal Society of Chemistry, UK.

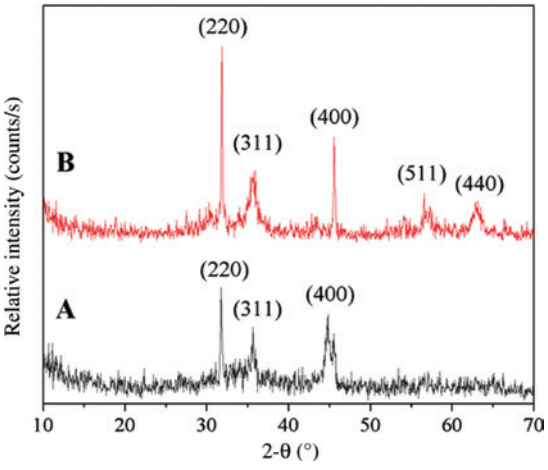

Figure 4: The powder X-ray diffraction (XRD) patterns of (A) CSMNPs and (B) the phytogenic magnetic nanoparticles (PMNPs). Reproduced from Ali et al. (2018) with permission from Royal Society of Chemistry, UK.

to NaCl as previously reported [18]. The fabricated PMNPs were highly crystalline. The majority of them indicated the sign of the magnetite/hematite NPs and they could be clearly assigned to the cube shape of metallic iron. The results of the XRD analysis show a series of high characteristic diffraction peaks at $2\theta = 32.5°$, 35.2°, 45.4°, 57.3° and 62.8°, respectively. These peaks were related to the (220), (311), (400), (511) and (440) planes of Fe_3O_4, as reported in the JCPD reference pattern 019-0629 [37]. The peaks at $2\theta = 35.2°$ and 62.8° mainly indicated the presence of iron oxide. The average diameter of the fabricated PMNPs was also calculated by using the Scherres equation expressed as $D = 0.89\lambda/\beta \cdot Cos\theta$, where D is the average particle size, λ is the wavelength of the CuKα irradiation, β is the full width at half maximum intensity of the diffraction peak and θ is the diffraction angle at $2\theta = 35.3°$ peak of the iron oxide NPs [34]. The fabricated PMNPs resulted in the mean crystallite size of ~39 nm. For comparison, the magnetic NPs (abbreviated herein as CSMNPs) were fabricated via the chemical co-precipitation method using sodium borohydrate ($NaBH_4$) as a reducing agent. The XRD pattern of the CSMNPs was also obtained and shown in Figure 4. A more or less similar XRD pattern was observed, which also verified that our fabricated PMNPs contained magnetite and hematite with crystalline shapes. In addition, the XRD pattern of the PMNPs also matched the standard data for the *Pisum sativum* peels extract of the Fe_3O_4 NPs (JCPDS no: 82-1533). These findings indicated that diffraction peak of our fabricated PMNPs was overlapping at $2\theta = 35.3°$, thus confirming the formation of the Fe_3O_4 NPs [31].

3.3.4 X-ray photoelectron spectrum (XPS) analysis

The XPS spectrum was obtained to understand the surface composition and structure of the fabricated PMNPs (Figure 5A). The XPS results clearly demonstrated three major peaks at 710.58/724.6, 529.95, and 284.79 eV, matching Fe 2p, O 1s and C 1s, respectively. The high-resolution XPS spectra were also obtained to thoroughly investigate the structure of Fe_3O_4 (Figure 5B–D). Figure 5B shows two major peaks at 710.58 and 724.6 eV in the binding energy range of 700–740 eV, which were associated to Fe $2p_{3/2}$ and Fe $2p_{1/2}$, respectively, thus proving the formation/phase purity of Fe_3O_4. The binding energy resembling Fe $2p_{3/2}$ is typical for Fe in iron oxide/Fe_3O_4 and iron oxohydroxide. In addition, there was no satellite peak at or around 719 eV, which is a typical characteristic feature of the maghemite phase (i.e. γ-Fe_2O_3), indicating the phase purity of Fe_3O_4 [37–40]. The O 1s spectra showed a major peak at 529.95

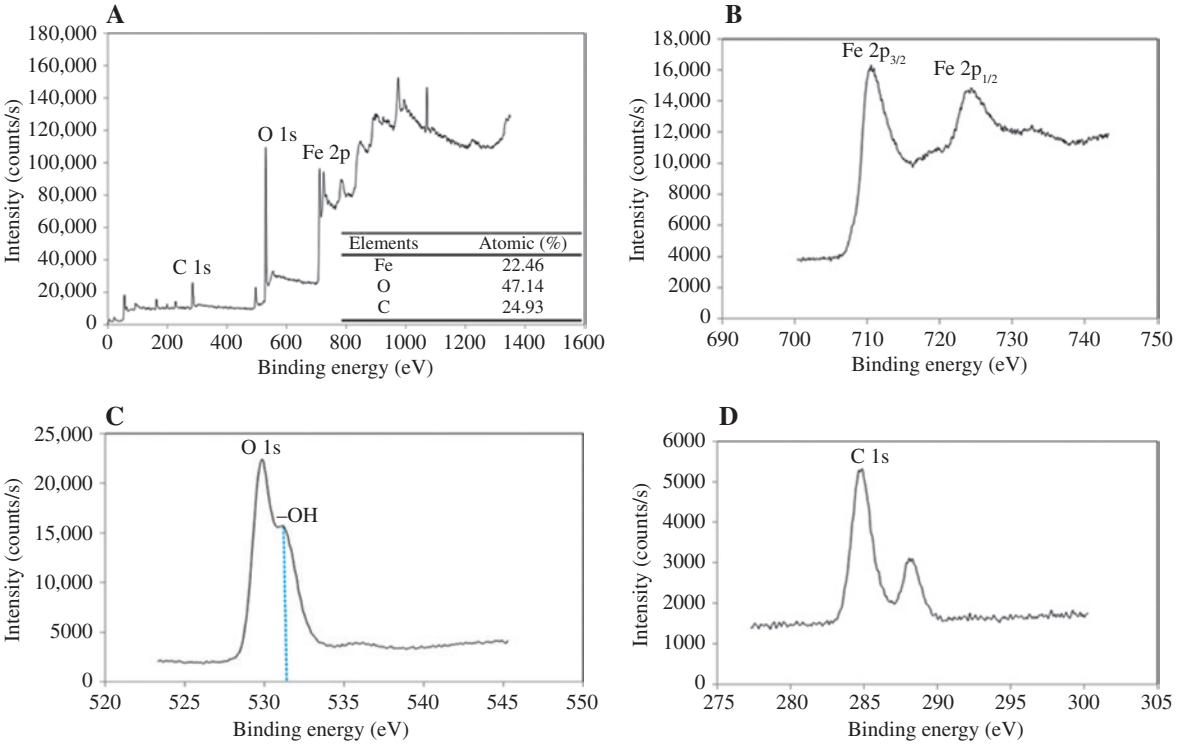

Figure 5: The X-ray photoelectron spectra (XPS) of (A) the phytogenic magnetic nanoparticles (PMNPs); (B) high-resolution X-ray photoelectron spectra (XPS) spectra of Fe 2p; (C) high-resolution XPS spectra of O 1s; (D) high-resolution XPS spectra of C 1s.

(~530) eV in addition to a small peak at 532.8 eV. The peak at 529.95 eV can be attributed to the lattice oxygen atoms bonding with Fe (Fe-O), whilst the peak at 532.8 eV can be assigned to O in the –OH groups of the PMNPs (Figure 5C). Moreover, the C 1s profile showed two peaks at 285.7 and 287.6 eV, respectively, in the bending energy range of 275–305 eV (Figure 5D). These features indicated the presence of two C atoms with different chemical characteristics. The main peak at 285.7 eV in C 1s can be assigned to the polyphenolic (O-H) or alcoholic (C-O) groups, which might be associated to the capping membrane of the organic functional groups onto the PMNPs. Overall, the XPS results in addition to the FTIR and XRD results clearly confirmed the formation of the PMNPs.

3.3.5 SEM and energy dispersive X-ray (EDX/S) analyses

The SEM analysis of the fabricated PMNPs was carried out to observe their morphology. As shown in Figure 6, the PMNPs showed the Fe_3O_4 (magnetite) with a granular, homogenous, spherical-shaped structure with a diameter in the range of 30–80 nm. In addition, EDS/X analysis provided the qualitative and quantitative status of the elements, which may have affected the fabrication of NPs. Figures 6B and D show that the EDX spectrum contained intense peaks of Na, Cl and C in addition to Fe and O. The Na and Cl peaks might have originated from the NaOH and $FeCl_3$ precursors used in the fabrication of PMNPs. The C peak in case of PMNPs was mainly due to the polyphenol groups or other carbon-containing bio-molecules, which were present in the *F. chinensis Roxb* leaves extract (Figure 6D). These findings revealed that the atomic percentages, as obtained by EDX quantification, were Fe (35.12%), C (17.12%), O (45.09%), Na (1.68%) and Cl (0.98%). The higher percentages of C indicated the involvement of the plant's bio-molecules in the reduction of metal ions and stabilisation of the PMNPs (Figure 6). Moreover, these values might be helpful in observing the atomic content on the surface and the near surface region of the fabricated PMNPs.

3.3.6 TEM analysis

The size, shape and morphological characteristics of the fabricated PMNPs were elucidated by TEM analysis. The TEM results were recorded at different scale bars. The

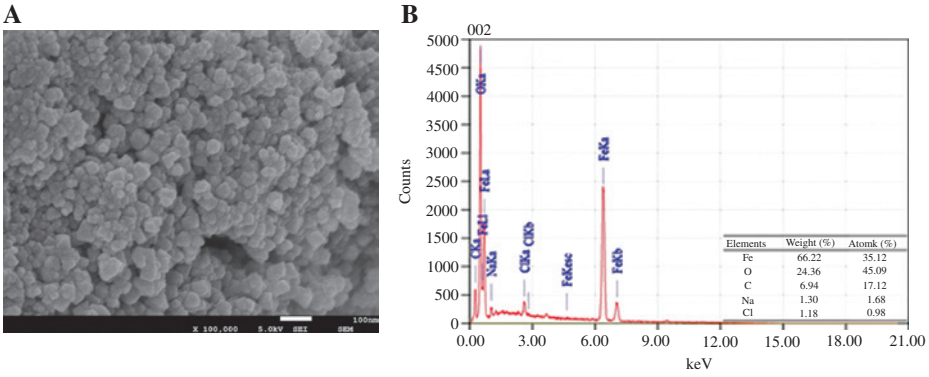

Figure 6: (A) The scanning electron microscopic (SEM) micrograph and (B) energy dispersive X-ray (EDX) spectra of the phytogenic magnetic nanoparticles (PMNPs).

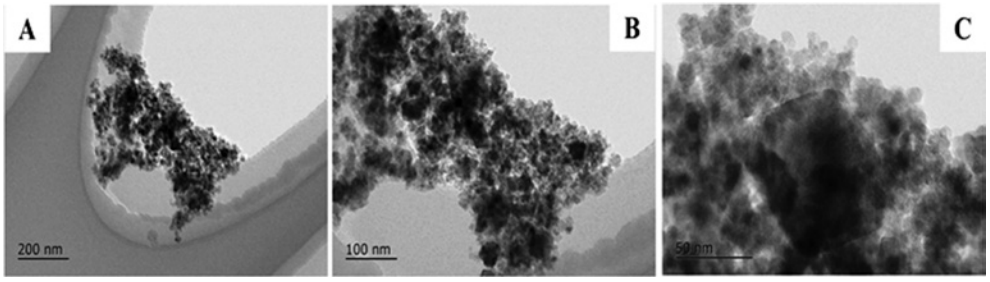

Figure 7: The transmission electron microscopy (TEM) images of the phytogenic magnetic nanoparticles (PMNPs); (A) 200 nm scale bar; (B) 100 nm scale bar; and (C) 50 nm scale bar.

results are shown in Figure 7. The TEM results clearly illustrated the formation of magnetite (Fe_3O_4) nanoparticles and the PMNPs with fine, monodisperse, compact and irregular shapes. The majority of them showed a cube-shaped morphology and some of them were spherical in shape. The average diameter of the majority of particles (e.g. >85% of PMNPs) ranged from 35 to 55 nm, which is in agreement with the results obtained from the powder XRD and SEM analyses (Figure 7). The particles were agglomerated due to the existence of the (–OH)/hydroxyl groups in the plant leaves extract. The surface of the PMNPs was coated by organic matters from the leaves extracts, which played an important role in restraining their aggregation and enhancing their dispersion and colloidal stability. In addition, the presence of high surface area and mesopore structure indicated that a large number of vacant/active sites could exist on the surface of PMNPs to adsorb heavy metal ions and toxic dyes from the aqueous environment (Figure 7). Overall, the TEM results clearly demonstrated the formation of the magnetite (Fe_3O_4) nanoparticles via the reduction of iron (Fe) ions within the leaves extract (Figure 7).

3.3.7 Brunauer-Emmet-Teller (BET) analysis

The surface properties of the PMNPs, such as surface area, total pore volume, pore radius and pore size, were also examined using the BET surface area analysis technique. Surface area is most often assumed as an important property of any material, which can disclose imperative information about the adsorption properties. A higher surface area is mostly desired over a lower one because the former offers high sorption capacity than the latter. A higher number of small sized pores is organised due to having a high surface area in a controlled volume. Similarly, the pore size of the material is an important element that reveals the availability of pollutants onto the particle surface. The N_2 adsorption-desorption method was employed to determine the surface properties of the PMNPs. The obtained isotherms showed a hysteresis loop of different intensities correlated with the type IV isotherm model with an H4-type hysteresis loop, as classified by the IUPC. The hysteresis loops took place at relative pressures between 0.46 and 0.99, and evoked the presence of the mesoporous feature of the sample (Figure 8). The specific surface area of the material was 54.916 m^2/g, as determined by the BET method. Surprisingly, the specific surface area of the PMNPs was much better than most of the previously reported green MNPs [14, 16, 19, 20, 29, 31, 38–41].

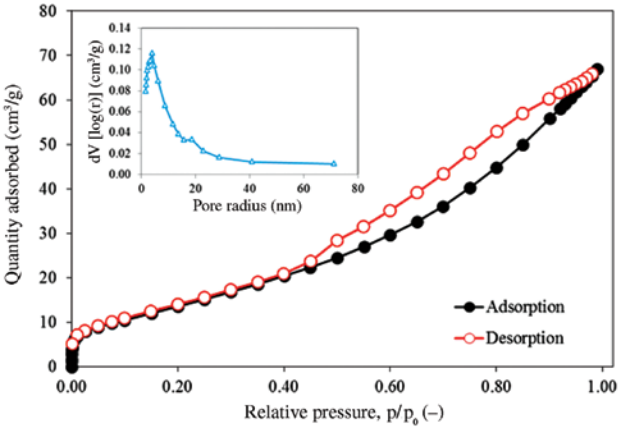

Figure 8: The N_2 adsorption-desorption isotherm at (77 K) pore size distribution (inset) of the phytogenic magnetic nanoparticles (PMNPs).

The Barrett-Joyner-Halenda (BJH) model was used to calculate average pore size and total pore volume. The results indicated that the average pore radius of the material ranged from 1.5 to 4.5 nm and the average pore size was 13.83 nm (the pictorial representation of the size distribution is shown in the inset of Figure 8). The total volume of the pores was determined by the single-point adsorption value at P/Po = 0.9989, which was 0.10 cm^3/g, indicating the presence of the loose mesoporous structure of the sample. Overall, the prepared material indicates the presence of mesoporosity, which can facilitate the diffusion of pollutants through the porous material. In addition, it can also facilitate in the adsorptive removal of toxic dyes and the separation of metal ions from the environment. The seporous magnetic materials can also be exploited as a catalyst and an adsorbent in various environmental and biomedical applications.

3.3.8 Magnetic measurements of the PMNPs

The magnetic nature is mainly dependent on size, shape and morphology of the prepared material, and are significantly influenced by the fabrication protocol. The VSM study was employed to obtain the hysteresis loop of the PMNPs at a temperature of 300 K by applying a magnetic field from –15 to +15kOe (Figure 9). The values of the remant magnetisation (Mr) and coercivity (Hc) was zero, suggesting the superparamagnetic nature of the PMNPs. Whilst the value of saturation magnetisation (Ms) was 50.95 emu/g. The lower value of Ms compared with Ms for bulk Fe_3O_4 = 93 emu/g, might be due to the increase in the surface area or the reactions among the organic capping agents and the

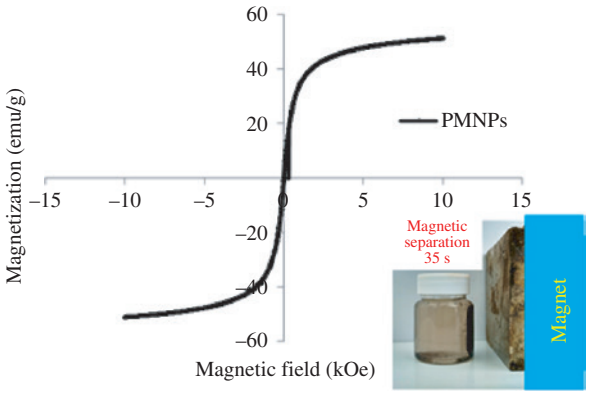

Figure 9: The M-H hysteresis loop/vibrating sample magnetometer (VSM) measurement of the phytogenic magnetic nanoparticles (PMNPs) at 300 K (the inset photo is the magnetic separation study of the PMNPs using a simple hand-held magnet; the distance between the magnet and the sample was 5 cm). Reproduced from Ali et al. (2018) with permission from Royal Society of Chemistry, UK.

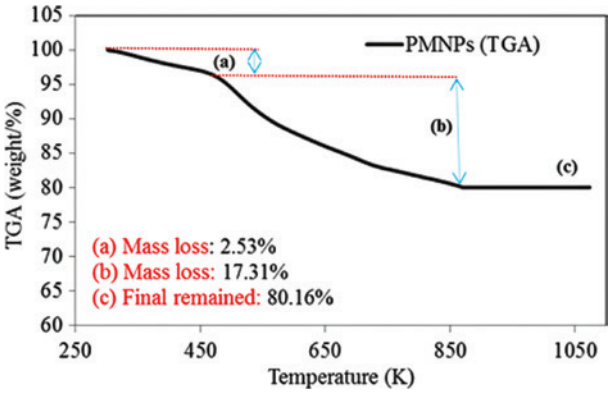

Figure 10: The thermal gravimetric analysis (TGA) plot/curve of the phytogenic magnetic nanoparticles (PMNPs). Reproduced from Ali et al. (2018) with permission from Royal Society of Chemistry, UK.

PMNPs. Similarly, the reduction in Ms values have also been reported by other researchers for green MNPs [28, 38–40]. Figure 9 illustrates that PMNPs can easily be separated from solution within a few seconds with the help of a hand-held magnet because of their superparamagnetic behaviour. Therefore, in order to improve operational efficiency and keep the treatment cost economically feasible, this material is perceived to be a prerequisite for the water/wastewater treatment process. The prepared material can be reused for consecutive treatment cycles and the recovery of metal ions. In addition, the developed material can be employed in biomedical applications (e.g. targeted gene and drug transportation) and the recovery of toxic heavy metals from the water environment.

3.3.9 Thermal gravimetric analysis (TGA)

The thermal stability and capping structure of the plant biomolecules and/or chemical composition of the PMNPs were estimated by using the TGA. The TGA plot/profile depicted two weight loss steps in the tested temperature range of 273.15 K–1073.15 K (Figure 10). The first mass/weight loss (2.53%) appeared in the temperature range of 301.15 K–576.45 K, indicating the removal of water/H_2O or residual solvent, physisorbed and chemisorbed H_2O molecules in the sample [28, 38–40]. The second major mass/weight loss (17.31%) occurred at 576.45 K–870.75 K, suggesting the elimination or decomposition/loss of the capping biomolecules [37, 42]. Further, there was no weight loss observed above 873.15 K and the PMNPs exhibited 80.16% remaining weight residue. The TGA results suggested that about 17% of the plant biomolecule capping was observed on the surface of the PMNPs and that the material possessed high thermal stability. The fabrication scheme of the PMNPs is shown in the Figure 11.

3.3.10 Decolourisation/degradation of toxic dyes at various operating conditions

Initially, the adsorbent dosages were varied to investigate the removal performance of the PMNPs against the selected toxic dyes (i.e. MG, CV and MB, in Figure 12A) The dosages of the PMNPs (0.05–1.5 g/l) were added into the 40 ml of toxic dye solution (25 mg/l) for 3 h at pH 6.5 (Figure 12A). The results indicated that the removal efficiencies of dyes increased with the increase of the adsorbent dosage (from 0.05 to 1.5 g/l) and approached equilibrium at the adsorbent dosage of 0.3 g/l (Figure 12A). This increase in the removal efficiencies might be due to the availability of higher active/vacant sites on the surface of adsorbents at higher dosages. This finding is consistent with the published studies, in which conventional bentonite supported nanoscale zero-valent iron reduced azo dye methyl orange [43]. Overall, a plateau was established in the range of 0.3–1.5 g/l, suggesting the equilibrium between the dye molecules and adsorbents (Figure 12A). Thereafter, a 0.3 g/l adsorbent dosage was added into the 40 ml dye solution (25 mg/l) at pH 6.5 to check the influence of contact time (Figure 12B). The finding indicated that PMNPs showed good reactivity against all the tested dyes and achieved greater than 95% removal efficiency within the contact time of 200 min. The MG and CV dyes almost disappeared completely after the contact time of 60 min and showed removal efficiencies about 99.12% and 98.23%, respectively

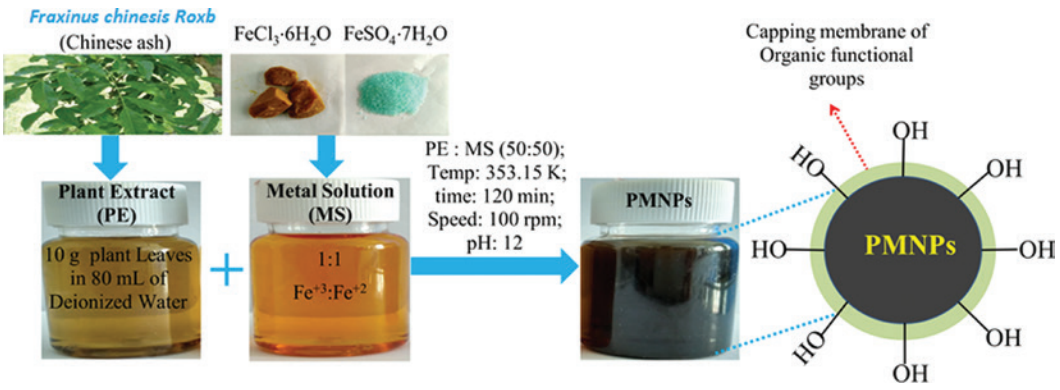

Figure 11: The fabrication scheme of the phytogenic magnetic nanoparticles (PMNPs). Reproduced from Ali et al. (2018) with permission from Royal Society of Chemistry, UK.

(Figure 12B). In contrast, almost a complete removal of MB (97.52%) was recorded within 200 min. This fast kinetics of the PMNPs against the dyes may indicate the presence of both adsorption (owing to the presence of hydroxyl/$-O^-$ functional groups on the surface of adsorbents) and oxidation mechanism (owing to the corrosion of iron/Fe in the solution). A fast removal of dyes happened in the starting phase due to the availability of higher active sites on the exterior surface of the PMNPs; afterwards, the dissolution of PMNPs led to the oxidation phenomenon. This finding agrees with the reports, which stated that iron oxides were impregnated onto the activated maize cob powder used to remove cationic dye [44].

Further, the removal of the dyes was also investigated in the range of pH 2–12 (Figure 12D). The results indicated that the removal efficiencies of all the three tested dyes increased with the increase of pH value, and minimum removal (<50%) was noticed in the pH range of 2–5 (Figure 12D). This might be due to the following reasons: first, the low solution pH favoured the corrosion of Fe° to form maghemite, magnetite and iron hydroxide on the surface of PMNPs, which in turn led to the inhibition of the removal of the dyes; second, at a lower pH, the solution made enough H^+ ions while deprotonating the MG molecules, which created competition to capture active sites that led to minimise removal efficiency; and finally, the pH_{PZC} of PMNPs was 6.19 (Figure 12C), at lower pH, when pH <.pH_{PZC} the surface of the PMNPs was positively charged, thus increasing the electrostatic repulsion between the cationic pollutants and the presence of proton (H^+) and protonated dyes molecules, consequently inhibiting the removal performance. In contrast, whilst in the alkaline solution, the surface of PMNPs was negatively charged at pH >.pH_{PZC}, and contained a large number of hydroxyl groups (–OH), which permitted the attachment of cationic dye ions with negatively charged adsorbent surface, thud leading to a higher removal capacity.

The influence of the initial concentration of dyes on the removal performance was also investigated by adding 0.3 g/l adsorbent dosage into the 40 ml dye solution (25–1000 mg/l) at pH of 6.5 (Figure 12E). The removal percentages of all three dyes were reduced (from 99.12% to 19.2%) by increasing the concentration from 25 to 1000 mg/l (Figure 12E). This is a general phenomenon, wherein increasing the initial concentration of pollutants leads to a competition between the adsorbates and adsorbents, when the active sites of the adsorbents are fixed [43]. The removal of 25 mg/l dyes by the PMNPs (0.3 g/l) at various reaction temperatures (298.15, 303.15, 313, 323.15 and 333.15 K) was tested to investigate the influence of temperature (Figure 12F). The results indicated that the removal efficiency of all the selected dyes increased with the increase of reaction temperature. An increment of about 1%–2% was observed in the removal efficiencies by increasing reaction temperature from 298.15 to 333.15 K (Figure 12F). Hence, the reaction temperature served as an important factor that increased the tendency of dyes molecules to transfer from the solution phase to the adsorbent surface (Figure 12F).

3.3.11 Proposed decolourisation/degradation mechanism of toxic dyes by the PMNPS

In order to understand the removal/degradation mechanism of the cationic toxic dyes by the PMNPs, the UV-vis spectra of MG, CV and MB were carried out at various time intervals (Figure 13). The absorption rates of the visible bands at 617, 425 and 311 nm significantly declined or disappeared within 60 min, when the PMNPs were mixed in the solution containing the MG dye (Figure 13A). Similarly,

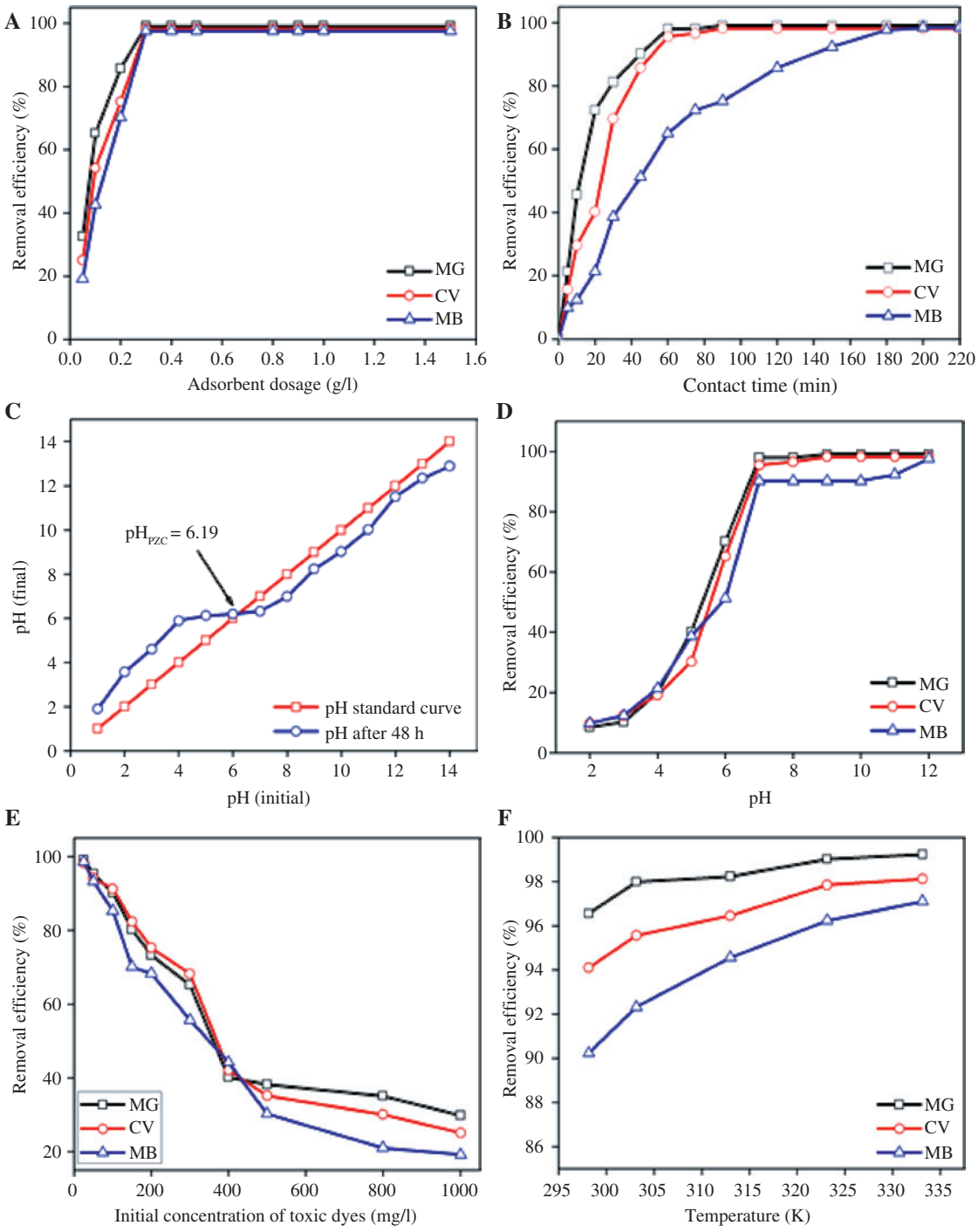

Figure 12: The removal/degradation of malachite green (MG), crystal violet (CV) and methylene blue (MB) at various operating conditions. (A) Effects of the adsorbent dosages: C_o = 25 mg/l, pH = 6.5, Temp = 298.15 K, dosages = 0.05–1.5 g/l and contact time = 3 h; (B) effects of contact time: C_o = 25 mg/l, pH = 6.5, Temp = 298.15 K and dosages = 0.3 g/l; (C) pH_{PZC} of the phytogenic magnetic nanoparticles (PMNPs); (D) effects of the solution pH: C_o = 25 mg/l, pH = 2–12, Temp = 298.15 K and dosages = 0.3 g/l; (E) effects of the initial concentration of toxic dyes: C_o = 25–1000 mg/l, pH = 6.5, Temp = 298.15 K and dosages = 0.3 g/l; and (F) effects of the reaction temperatures: C_o = 25 mg/l, pH = 6.5, Temp = 298.15–333.15 K and dosages = 0.3 g/l.

the absorption rates of the visible bands for the CV dye at 585, 291 and 239 nm significantly reduced within 60 min (Figure 13B). In contrast, the absorption rates of the visible band for the MB dye at 664, 290 and 242 nm gradually declined within the contact time of 200 min (Figure 13C). This decline or disappearance of visible bands (when the

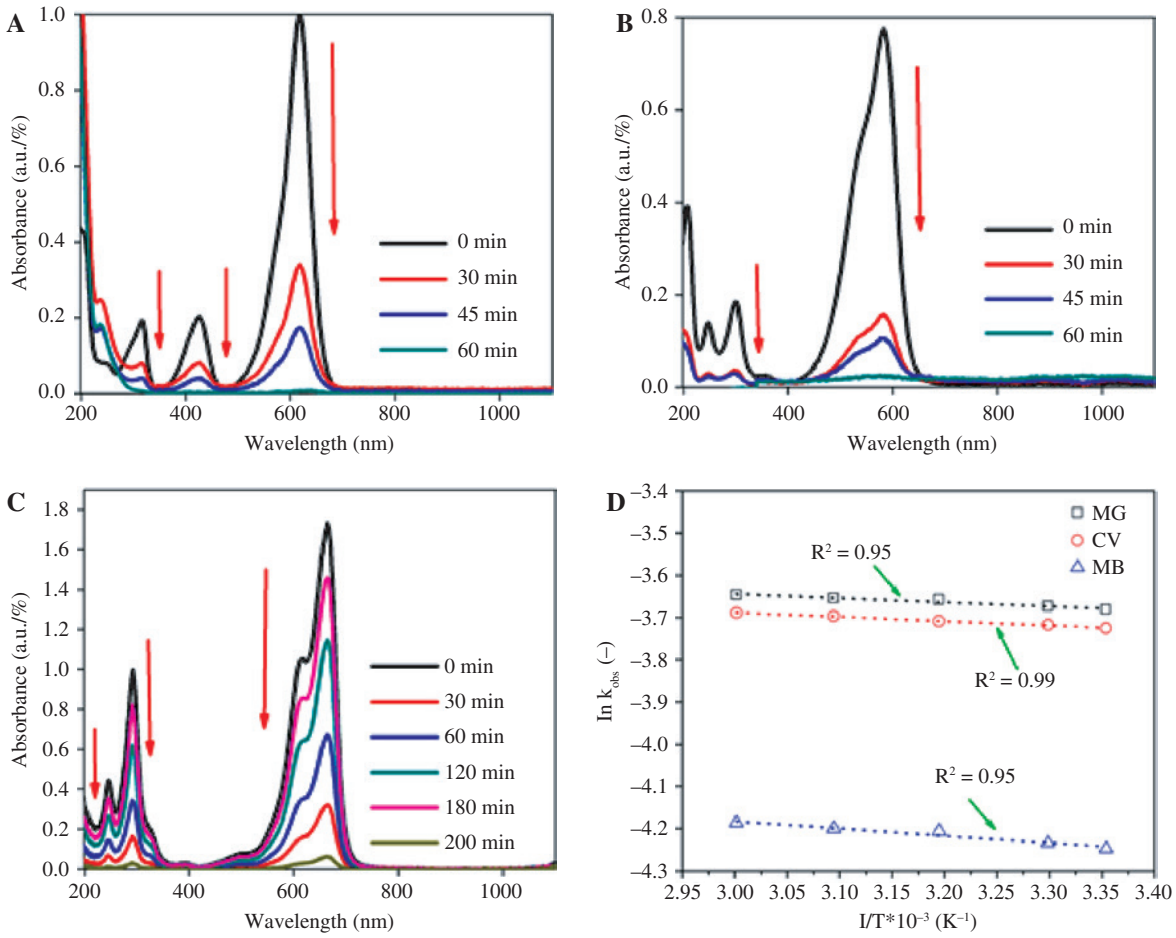

Figure 13: The UV–vis spectra of the degradation of (A) malachite green (MG), (B) crystal violet (CV) and (C) methylene blue (MB) dyes using the phytogenic magnetic nanoparticles (PMNPs) at various times; and (D) linear plots of $\ln K_a$ against 1/T for the degradation of the MG, CV and MB dyes by the PMNPS at various reaction temperatures.

reaction time increased) indicated that the entire conjugated chromophore structure of the cationic toxic dyes had been abolished/destroyed or the cationic ions had been adsorbed onto the surface of the PMNPs [45]. In addition, these findings indicate that the removal of these cationic toxic dyes by the PMNPs was due to the adsorption of the dye molecules onto the surface of adsorbents and the cleaving of the -C=C- and =C=N- bonds of MG, CV and MB, respectively, suggesting that the removal of cationic toxic dyes by PMNPs could include both the adsorption and degradation/oxidation processes. The adsorption of the cationic dyes occurred mainly due to the presence of hydroxyl/–OH functional groups/organic capping agents on the surface of the PMNPs, and following the degradation of these dyes by the corrosion of Fe° in the solution occurred. These degraded products at 200–220 nm could be linked to the aromatic ring [46]. Overall, the absorption of the visible bands for MG, CV and MB was rapidly declined/abated by the PMNPs due to its higher reactivity. These findings are consistent with the results described in the published literature [14, 18–20, 35, 43].

Furthermore, to better understand the degradation mechanism, the pseudo-first order kinetics model was employed to check the degradation of the MG, CV and MB dyes by the PMNPs. This can be explained as [47]

$$\ln\frac{c}{c_o} = (-k_{obs}t),$$

where C_o (mg/l) is the initial concentration of the dye solution, C (mg/l) is the final concentration of the dye in the solution, t (min) is the time interval and k_{obs} is the rate constant of a pseudo-first order reaction (min^{-1}), which can be estimated from the slope of the line by plotting $\ln(c/c_o)$ versus t. As shown in Table 2, the plots of $\ln(c/c_o)$ versus t were linear with a high correlation coefficient ($R^2 > 0.90$) at various reaction temperatures (i.e. 298.15, 303.15, 313, 323.15 and 333.15 K). The results suggested that the removal rates of the MG, CV and MB dyes by the PMNPs

Table 2: The pseudo-first order kinetic parameters for the degradation of malachite green (MG), crystal violet (CV) and methylene blue (MB) dyes by the phytogenic magnetic nanoparticles (PMNPs) at various reaction temperatures.

Temperature (K)→ Parameters ↓	298.15	303.15	313	323.15	333.15
MG					
R^2	0.92	0.93	0.93	0.93	0.93
k_{obs}	0.0252	0.0254	0.0258	0.0259	0.0261
Ea (kJ/mol)					97.623
CV					
R^2	0.94	0.94	0.94	0.94	0.93
k_{obs}	0.0241	0.0243	0.0245	0.0248	0.0250
Ea (kJ/mol)					102.59
MB					
R^2	0.96	0.96	0.96	0.96	0.97
k_{obs}	0.0143	0.0145	0.0149	0.0150	0.0152
Ea (kJ/mol)					169.76

matched well to a pseudo-first order kinetics model. The summary of the calculated rate constants and correlation coefficients is documented in Table 2.

In addition, the apparent activation energy was also estimated by the equation [19, 20, 45]

$$\ln k_{obs} = -\frac{E_a}{RT} + \ln A_o,$$

where R (J/mol K) is the universal gas constant, T(K) is the reaction temperature, E_a (kJ/mol) is the apparent activation energy and A_o is the pre-exponential factor with the same dimension as k_{obs}, and it can be estimated through the slope and intercept by plotting $\ln K_a$ against 1/T (Figure 13D). The degradation/apparent activation energies of the MG, CV and MB dyes by the PMNPs were estimated to be 97.623, 102.59 and 169.76 kJ/mol, respectively (Table 2). These values suggested that, chemically speaking, a diffusion-controlled reaction did occur in the removal/degradation of cationic toxic dyes using the PMNPs [19, 20, 47]. As shown in Figure 13D, the regression coefficient (R^2) values of the MG, CV and MB dyes were greater than 0.90 at various reaction temperatures, indicating that the removal rate fitted well to a pseudo-first order kinetics model. Therefore, the reaction was kinetically favourable to the PMNPs. Altogether, the pathway for the removal/degradation of the MG, CV and MB dyes in the aqueous solution using the PMNPs can be described as follows: (a) first, the cationic toxic dyes were adsorbed onto the surface of PMNPs owing to presence of the negative charged hydroxyl/$-O^-$ functional groups on the surface of the adsorbent; (b) second, the PMNPs in the aqueous solution were corroded/dissolved, which released electrons that cleaved the -C=C- and =C=N- bonds linked to the benzene ring of the MG, CV and MB dyes, respectively, thus degrading the dyes through the oxidation mechanism. These processes can be described below [14, 19, 20, 35, 46, 48, 49].

(a) Adsorption process
$MG/CV/MB + PMNPs \rightarrow MG/CV/MB - PMNPs$

(b) The corrosion of Fe/PMNPs in the solution
$Fe°/PMNPs + 2H_2O \rightarrow Fe^{2+} + 2OH^- + H_2$ (in alkaline/basic solution/environment)
$Fe°/PMNPs + 2H+ \rightarrow Fe^{2+} + H_2$ (in acidic solution/environment)

(c) Cleaving the bond that was connected to the benzene ring
$H_2 + MG/CV/MB \rightarrow [MG/CV/MB]_{reduced}$

Finally, compared with other green magnetic sorbents for the removal/degradation of toxic dyes from wastewater, it can be observed that the PMNPs had comparatively much

Table 3: Comparison of the phytogenic magnetic nanoparticles (PMNPs) removal/degradation performance with the other reported green magnetic adsorbents employed for the degradation of the cationic toxic dyes from the aqueous solution.

Cationic toxic dyes	Adsorbent	Removal/degradation efficiency (%)	Reaction time (min)	References
MG	Black tea extract-fabricated green MNPs	67.1	60	[20]
MG	Oolong tea extract-fabricated green MNPs	75.5%	60	[20]
MG	Oolong tea extract-fabricated green MNPs	75.6	60	[19]
MG	Green tea extract-fabricated green MNPs	81.2	60	[20]
MG	GT-Fe NPs/green tea extract-fabricated green MNPs	96	60	[41]
MG	PMNPs/*Fraxinus chinensis Roxb leaves* extract-fabricated green MNPs	99.12	60	Present study
MB	Ridge gourd peels (RG) extract fabricated green MNPs	96	30	[14]
MB	Homemade starch-rich potato extract-fabricated green MNPs	96.56	30	[35]
MB	Green tea leaves extract-fabricated green MNPs	99.97	200	[18]
MB	PMNPs/*Fraxinus chinensis Roxb leaves* extract-fabricated green MNPs	97.52	200	Present study
CV	PMNPs/*Fraxinus chinensis Roxb leaves* extract-fabricated green MNPs	98.23	60	Present study

better degradation performance against the MG, CV and MB dyes (Table 3). Moreover, an eco-friendly fabrication process, wide operable pH range, and the rapid and easy magnetic separation from the final effluents just by applying simple hand-held magnet makes PMNPs an attractive candidate for the treatment of wastewaters containing cationic toxic dyes. The fabricated PMNPs in the current research can provide broad applications in the fields of green chemistry and environmental engineering.

4 Conclusions

In the present research, innovative super paramagnetic PMNPs were fabricated by employing non-toxic, cheap and environmental friendly "green" recipe using the *F. chinensis Roxb* leaves extract as a reducing and capping agent. The developed methods did not require any additional toxic or hazardous chemicals and can be scaled up for bulk production and use. The formation of the PMNPs was characterised with the help of different techniques (i.e. UV-visible spectrometry, FTIR, powder XRD, SEM, EDX, TEM, VSM, XPS, BET and TGA).

The results showed that the best plant extraction conditions were observed at pH 3, temperature (353.15 K), contact time (90 min) and 10 g mass of plant leaves per 80 ml of solvent. The FTIR and TGA results verified the capping and involvement of the plant bio-molecules on the surface of the PMNPs in the form of the -OH, C-H, C-O functional groups. The hysteresis loops of the PMNPs showed an excellent super paramagnetic nature with a saturation magnetisation value of 50.95 emu/g and offered the fastest separation time of 35 s from the aqueous solutions. The SEM results illustrated that the PMNPs mainly showed a granular, homogenous and porous spherical-shaped structure of Fe_3O_4 (magnetite) with a diameter ranging from 30 to 80 nm. The TEM results further demonstrate that the PMNPs (d = 35–55 nm) can be fabricated using the tree leaf extract of *F. chinensis Roxb*. The powder XRD and XPS analyses revealed that the produced PMNPs were magnetite and clearly assigned to the cube shape of metallic iron. The specific surface area of the material was 54.916 m^2/g, as determined by the BET method, and the results showed the presence of a loose mesoporous structure of the PMNPs.

Meanwhile, the TGA results revealed that the material was thermally stable and exhibited 80.16% weight residue. Moreover, the findings depicted that the PMNPs could remove about 99.12% of MG, 98.23% of CV and 97.52% of MB with a concentration of 25 mg/l at a temperature of 298.15 K and pH 6.5, using the PMNP dosage of 0.3 g/l. The kinetics indicated that the degradation of the MG, CV and MB dyes by the PMNPs fitted well to the pseudo first-order reaction kinetics model. Moreover, the estimated apparent activation energies for such dyes were more than 20 kJ/mole, suggesting a chemical, diffusion-controlled reaction. Further, the findings showed that the degradation mechanisms of the MG, CV and MB dyes by the PMNPs included the adsorption of the cationic dyes molecules onto the negatively charged surface of the adsorbent, oxidation or corrosion of iron/Fe° and the cleaving of the bonds associated to the benzene ring. Overall, the fabricated PMNPs can be produced in bulk scale and have the potential as a green/biocompatible/non-toxic nanomaterial for biomedical and environmental remediation purposes.

Acknowledgments: This work was supported by the State Key Laboratory of Environmental Criteria and Risk Assessment (No. SKLECRA 2013FP12) and the Shandong Province Key Research and Development Program (No. 2016GSF115040). The first author would like to thank the financial support provided by the Chinese Scholarship Council, China (CSC No. 2016GXYO20).

References

[1] Su C. *J. Hazard. Mater.* 2017, 322, 48–84.
[2] Ali I, Peng C, Naz I, Khan ZM, Sultan M, Islam T, Abbasi IA. *RSC Adv.* 2017a, 7, 40158–40178.
[3] Ali I, Peng C, Khan ZM, Naz I. *J. Basic Microbiol.* 2017b, 57, 643–652.
[4] Nadagouda MN, Castle AB, Murdock RC. *Green Chem*. 2010, 12, 114–122.
[5] Ali I, Peng C, Ye T, Naz I. *RSC Adv.* 2018, 8, 16, 8878–8897.
[6] Sivashankar R, Sathya AB, Vasantharaj K, Sivasubramanian V. *ENMM* 2014, 1, 36–49.
[7] Rahimi-Nasrabadi M, Ahmadi F, Eghbali-Arani M. *J. Mater. Sci. Mater. Electron.* 2016, 27, 11873–11878.
[8] Ahmadi F, Rahimi-Nasrabadi M, Fosooni A, Daneshmand M. *J. Mater. Sci. Mater. Electron.* 2016, 27, 9514–9519.
[9] Rahimi-Nasrabadi M. *J. Mater. Sci. Mater. Electron*. 2017, 28, 2200–2205.
[10] Sobhani-Nasab A, Naderi H, Rahimi-Nasrabadi M, Ganjali MR. *J. Mater. Sci. Mater. Electron.* 2017, 28, 8588–8595.
[11] Rahimi-Nasrabadi M, Behpour M, Sobhani-Nasab A, Hosseinpour-Mashkani SM. *J. Mater. Sci. Mater. Electron.* 2015, 26, 9776–9781.
[12] Djahaniani H, Rahimi-Nasrabadi M, Saiedpour M, Nazarian S, Ganjali M, Batooli H. *Int. J. Food Prop.* 2017, 20, 922–930.
[13] Mystrioti C, Sparis D, Papasiopi N, Xenidis A, Dermatas D, Chrysochoou M. *Bull. Environ. Contam. Toxicol*. 2015, 94, 302–307.
[14] Cheera P, Karlapudi S, Sellola G, Ponneri V. *J. Mol. Liq.* 2016, 221, 993–998.

[15] Moulton MC, Braydich-Stolle LK, Nadagouda MN, Kunzelman S, Hussain SM, Varma RS. *Nanoscale* 2010, 2, 763–770.
[16] Abbassi R, Yadav AK, Kumar N, Huang S, Jaffe PR. *Ecol. Eng.* 2013, 61, 366–370.
[17] Machado S, Pinto SL, Grosso JP, Nouws HPA, Albergaria JT, Delerue-Matos C. *Sci. Total Environ.* 2013, 445, 1–8.
[18] Shahwan T, Sirriah SA, Nairat M, Boyacı E, Eroğlu AE, Scott TB, Hallam KR. *Chem. Eng. J.* 2011, 172, 258–266.
[19] Huang L, Weng X, Chen Z, Megharaj M, Naidu R. *Spectrochim Acta. A. Mol. Biomol. Spectrosc.* 2014a, 117, 801–804.
[20] Huang L, Weng X, Chen Z, Megharaj M, Naidu R. *Spectrochim Acta. A. Mol. Biomol. Spectrosc.* 2014b, 130, 295–301.
[21] Machado S, Pacheco JG, Nouws HPA, Albergaria JT. *Sci. Total Environ.* 2015, 533, 76–81.
[22] Nadagouda MN, Varma RS. *Green Chem.* 2008, 10, 859–862.
[23] Fazlzadeh M, Rahmani K, Zarei A, Abdoallahzadeh H, Nasiri F, Khosravi R. *Adv. Powder Technol.* 2017, 28, 122–130.
[24] Gupta VK, Nayak A. *Chem. Eng. J.* 2012, 180, 81–90.
[25] Lingamdinne LP, Chang YY, Yang JK, Singh J, Choi EH, Shiratani M, Attri P. *Chem. Eng. J.* 2017, 307, 74–84.
[26] Martínez-Cabanas M, López-García M, Barriada JL, Herrero R, de Vicente MES. *Chem. Eng. J.* 2016, 301, 83–91.
[27] Prasad KS, Gandhi P, Selvaraj K. *Appl. Surf. Sci.* 2014, 317, 1052–1059.
[28] Venkateswarlu S, Kumar BN, Prathima B, Subba Rao Y, Jyothi NVV. *Arab J. Chem.* 2014 (in press). Available at: http://dx.doi.org/10.1016/j.arabjc.2014.09.006.
[29] Venkateswarlu S, Lee D, Yoon M. *ACS Appl. Mater. Interfaces.* 2016, 8, 23876–23885.
[30] Shamaila S, Sajjad AKL, Farooqi SA, Jabeen N, Majeed S, Farooq I. *Appl. Mater. Today.* 2016, 5, 150–199.
[31] Venkateswarlu S, Kumar BN, Prasad CH, Venkateswarlu P, Jyothi NVV. *Physica. B. Condens. Matter.* 2014b, 49, 67–71.
[32] Manquián-Cerda K, Cruces E, Rubio MA, Reyes C, Arancibia-Miranda N. *Ecotoxicol. Environ. Saf.* 2007, 145, 69–77.
[33] Smuleac V, Varma R, Sikdar S, Bhattacharyya D. *J. Membr. Sci.* 2011, 379, 131–137.
[34] Wei Y, Fang Z, Zheng L, Tsang EP. *Appl. Surf. Sci.* 2017, 399, 322–329.
[35] Buazar F, Baghlani-Nejazd MH, Badri M, Kashisaz M, Khaledi-Nasab A, Kroushawi F. *Starch/Stärke* 2016, 68, 796–804.
[36] Prasad C, Yuvaraja G, Venkateswarlu P. *J. Magn. Magn. Mater.* 2017, 424, 376–381.
[37] Burks T, Avila M, Akhtar F, Göthelid M, Lansåker PC, Toprak MS, Muhammed M, Uheida A. *J. Colloid. Interface Sci.* 2014, 425, 36–43.
[38] Venkateswarlu S, Yoon M. *ACS Appl. Mater. Interfaces* 2015a, 7, 25362–25372.
[39] Venkateswarlu S, Kumar SH, Jyothi NVV. *Water Resour. Ind.* 2015b, 12, 1–7.
[40] Venkateswarlu S, Minyoung Y. *Dalton. Trans.* 2015c, 44, 18427–18437.
[41] Weng X, Huang L, Chen Z, Megharaj M, Naidu R. *Ind. Crops. Prod.* 2013, 51, 342–347.
[42] Morillo D, Uheida A, Pérez G, Muhammed M, Valiente M. *J. Colloid. Interface. Sci.* 2015, 438, 227–234.
[43] Chen ZX, Jin XY, Chen ZL, Megharaj M, Naidu R. *J. Colloid Interface Sci.* 2011, 363, 601–607.
[44] Tan KA, Morad N, Teng TT, Norli I, Panneerselvam P. *APCBEE Proced.* 2012, 1, 83–89.
[45] Lin YM, Chen ZL, Megharaj M, Naidu R. *J. Colloid Interface Sci.* 2012, 381, 30–35.
[46] Kumar KM, Mandal BK, Kumar KS, Reddy PS, Sreedhar B. *Spectrochim. Acta A.* 2013, 102, 128–133.
[47] Bokare AD, Chikate RC, Rode CV, Paknikar KM. *Appl. Catal. B Environ.* 2008, 79, 270–278.
[48] Hoag GE, Collins JB, Holcomb JL, Hoag JR, Nadagouda MN, Varma RS. *J. Mater. Chem.* 2009, 19, 8671–8677.
[49] Nadagouda MN, Castle AB, Murdock RC, Hussain SM, Varma RS. *Green Chem.* 2010, 12, 114–122.